PNAS
www.pnas.org

Supplementary Information for

Polar vacuolar distribution is essential for accurate asymmetric division of *Arabidopsis* zygotes

Yusuke Kimata, Takehide Kato, Takumi Higaki, Daisuke Kurihara, Tomomi Yamada, Shoji Segami, Miyo Terao Morita, Masayoshi Maeshima, Seiichiro Hasezawa, Tetsuya Higashiyama, Masao Tasaka and Minako Ueda

Minako Ueda
Email: m-ueda@itbm.nagoya-u.ac.jp

This PDF file includes:

Supplementary text
Figs. S1 to S4
Captions for movies S1 to S4
References for SI reference citations

Other supplementary materials for this manuscript include the following:

Movies S1 to S4

www.pnas.org/cgi/doi/10.1073/pnas.1814160116

Supplementary Materials and Methods

Strains and growth conditions

All *Arabidopsis* lines were in the Columbia (Col-0) background. The *sgr2-1* and *sand-2* (GABI_397H04) mutants were described previously (1, 2). The *tpc1-2* (SALK_145413) (3), *tip1;3-1* (SALK_088276) (4), *tip3;1* (SALK_053807) (5), *nhx1-2* (SALK_065623) (6) and *nhx2-1* (SALK_036114) (6) were obtained from SALK Institute. Plants were grown at 18–22°C under continuous light or long-day conditions (16-h light/8-h dark).

Plasmid construction for transgenic plants

The vacuolar/nuclear marker for egg cell and zygote contains EC1p::VHP1-mGFP (coded as MU1980) as vacuolar membrane marker, and EC1p::H2B-tdTomato and DD22p::H2B-mCherry (coded as MU1968) as nuclear markers. In EC1p::VHP1-mGFP, the 463-bp EGG CELL1 (EC1) promoter (7) was fused to monomeric GFP (mGFP), the full-length coding region of vacuolar proton pump (VACUOLAR H^+-PPASE; VHP1; AT1G15690) (8), and NOPALINE SYNTHASE (NOS) terminator in a pAlligator-derived binary vector (9). EC1p::H2B-tdTomato is an egg cell/zygote-specific nuclear marker, containing EC1 promoter, the full-length coding region of histone 2B (H2B; AT1G07790), red-fluorescent tandem dimer Tomato (tdTomato), and NOS terminator. DD22p::H2B-mCherry is a central cell/endosperm-specific nuclear marker, consisting of the 1.0-kb DOWNREGULATED IN DIF1 22 (DD22) promoter (10, 11), the full-length coding region of H2B, red-fluorescent mCherry, and NOS terminator. These markers were combined in pAlligator-derived binary vector. This construct was also combined to F-actin marker (EC1p::Lifeact-Venus; coded as MU1526) (9, 12) to generate the F-actin/nucleus marker.
The vacuolar/nuclear marker for later embryo imaging contains WOX2p::VHP1-mGFP (coded as MU2238) and WOX2p::H2B-tdTomato (coded as MU1934), in addition to the above EC1p::VHP1-mGFP, EC1p::H2B-tdTomato and DD22p::H2B-mCherry. In WOX2p::VHP1-mGFP, the 3.5-kb WUS HOMEOBOX2 (WOX2) promoter (13) was fused to the VHP1-mGFP and NOS terminator in a pPZP221 binary vector (14). In WOX2p::H2B-tdTomato, WOX2 promoter was fused to H2B-tdTomato and NOS terminator in pMDC123 binary vector (15).
The vacuolar/nuclear marker for root and root hair contains VHP1p::VHP1-mGFP, which was previously described (8), and RPS5Ap::H2B-tdTomato (coded as MU1164). In RPS5Ap::H2B-tdTomato, WOX2 promoter in WOX2p::H2B-tdTomato was replaced by the 1.7-kb RIBOSOMAL PROTEIN SUBUNIT 5A (RPS5A) promoter (16).
The vacuolar lumen marker for vacuole morphometry is EC1p::SP-mTur2-CTPP (coded as MU2125), containing EC1 promoter, cyan-fluorescent mTurquoise2 (mTur2) that fused to the signal peptide (SP) sequence of ENDOXYLOGLUCAN TRANSFERASE-A1 (EXGT-A1; AT2G06850) at N-terminus and to a vacuolar sorting signal COOH-terminal propeptide (CTPP) (17) at C-terminus, and NOS terminator in a pMDC123 binary vector.
The F-actin/vacuolar lumen marker contains EC1p::Lifeact-mNeonGreen (coded as MU2232) and EC1p::SP-mScarlet-I-CTPP (coded as MU2256). In EC1p::Lifeact-mNeonGreen, EC1 promoter, green-fluorescent mNeonGreen that fused to Lifeact sequence from EC1p::Lifeact-Venus, and NOS terminator were combined in a pMDC99 binary vector (15). In EC1p::SP-mScarlet-I-CTPP, mTur2 in EC1p::SP-mTur2-CTPP was replaced by red-fluorescent mScarlet-I. These constructs were transformed into *Arabidopsis* using floral dip method (18).

Histological analysis and microscopy

In vitro ovule cultivation and zygote imaging were performed as previously described (12, 19). The 2PEM images were acquired using a laser-scanning inverted microscope (A1R MP; Nikon) equipped with a Ti:sapphire femtosecond pulse laser (Mai Tai DeepSee; Spectra-Physics). All images were acquired with excitation at 950 nm, only except for the F-actin/vacuolar lumen

marker, whose images were acquired at 1000 nm. The images of eight-cell stage embryos and zygotes were acquired using a 25× water-immersion objective lens (CFI Apo LWD 25x WI, NA = 1.10, WD = 2.00 mm; Nikon) and a 40× water-immersion objective lens (CFI Apo LWD WI, NA = 1.15, WD = 0.59–0.61 mm; Nikon), respectively, with Immersol W 2010 (Zeiss) immersion medium. Fluorescence signals were detected by external non-descanned GaAsP PMT detectors. We used two dichroic mirrors, DM495 and DM560, and three band-pass filters, 479/40 nm for mTur2, 534/30 nm for mGFP, Venus, and mNeonGreen, and 578/105 nm for tdTomato, mCherry, and mScarlet-I. Time-lapse images were taken at 31 z-stacks with 1-µm intervals every 20 min. Images for the quantitative analysis of F-actin and vacuole patterns were taken at 62 z-stacks with 0.5-µm intervals and 2× averaging. MIP was performed using NIS-Elements AR 4.10 software (Nikon) or ImageJ (http://rsbweb.nih.gov/ij/index.html).
For the confocal observation of root meristem and root hair, five-day-old seedlings were stained with 10 µg/ml propidium iodide (PI; Sigma), and observed using a laser-scanning inverted microscope (LSM780-DUO-NLO; Zeiss) with a 20× objective lens (20× Plan-Apo, NA = 0.80, WD = 0.55 mm; Zeiss). The emission signal of GFP was detected between 491 and 558 nm with 488 nm excitation, and that of PI/tdTomato was detected between 570 and 649 nm with 561 nm excitation.
For the sectional analysis of embryogenesis, resinous sections were prepared using Technovit 7100 (Heraeus Kulzer), and 4-µm sections were stained by Toluidine Blue O (TBO).
The DIC observation of the zygote and embryo was performed using cleared seeds in the following solution; 1:8:3 glycerin:chloral hydrate:water. For stomata observation, five-day-old cotyledons were fixed with 90% acetate and 10% ethanol for overnight, and then cleared in the same solution for seeds. DIC microscopy was performed using AxioImager A2 (Zeiss) with a 40× objective lens (40× Plan-Apo, NA = 0.95, WD = 0.25 mm; Zeiss), an AxioCam HRm camera (Zeiss), and AxioVision software (Zeiss).

Image quantification and 3D-reconstruction

For the measurements of the length of apical/basal regions, MIP images of nucleus marker were binarized (method = Otsu/Yen) after Gaussian filtering (sigma = 2 pixels), and then the distance between the nucleus center and the apical/basal tip was measured.
Vacuolar areas, perimeter, and circularity were measured based on the binary vacuole images that were obtained by the same method in nucleus image (Fig. S2B and C). Circularity was defined as $4\pi SL^{-2}$, where S and L represent the vacuole area and perimeter, respectively.
Quantification of F-actin pattern was performed as previously described (12, 20), and statistic analysis was done with Brunner–Munzel test (21).
All image quantifications were performed using ImageJ software (https://imagej.nih.gov/ij/index.html). The 3D surface reconstruction and visualization of the vacuole were performed using Imaris (Bitplane).

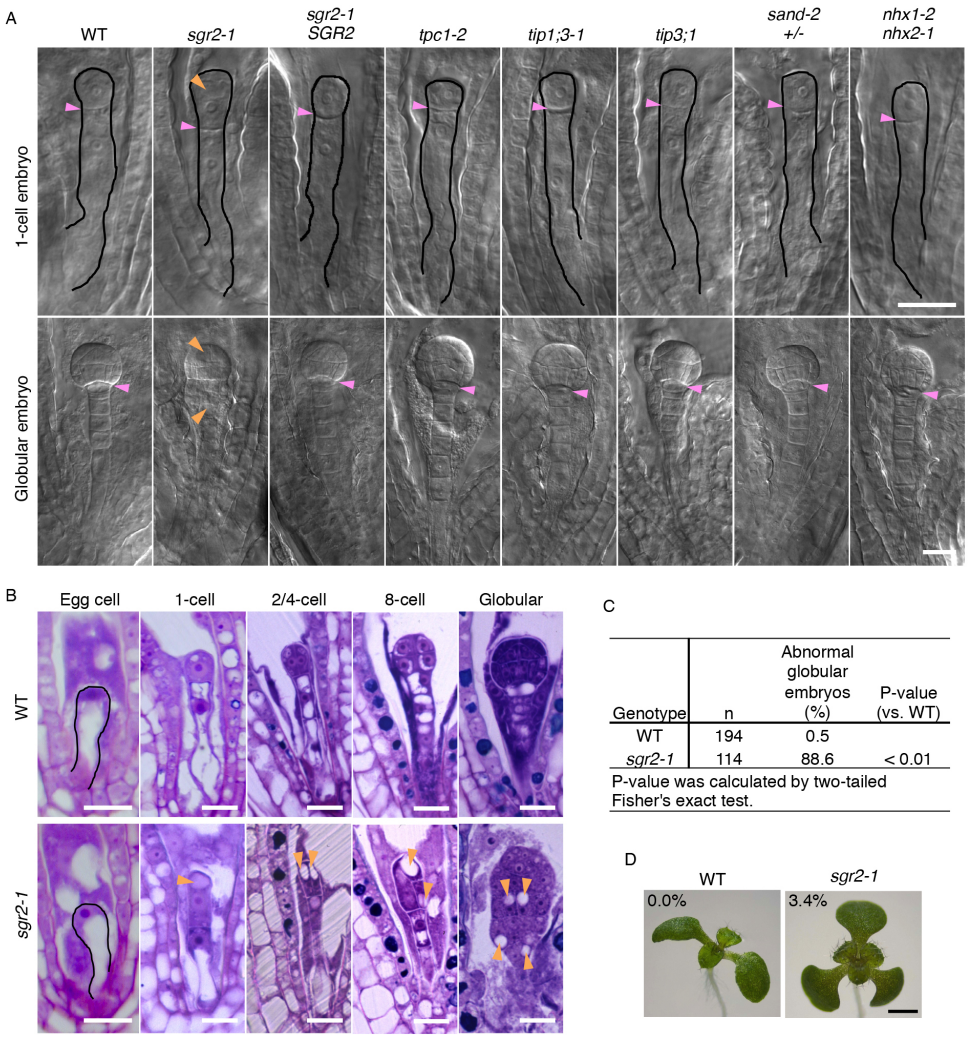

Fig. S1. Zygotic and embryonic phenotypes of vacuolar mutants.
(A) DIC images of cleared one-cell stage and globular embryos of the indicated genotypes. One-cell stage embryos are outlined. Magenta arrowheads indicate the cell division planes in one-cell stage embryos and the boundaries of embryo proper and suspensor in globular embryos. Note that the boundary in the globular embryo is unclear in *sgr2-1*. Orange arrowheads indicate apically-remaining large vacuoles. Indicated lines are as follows; wild type (WT), *shoot gravitropism2-1* (*sgr2-1*) that affects vacuole shape change, *sgr2-1* containing pSGR2::SGR2i-GFP transgene (*sgr2-1 SGR2*), *two-pore channel1-2* (*tpc1-2*) that lacks slow vacuolar channel activity, *tonoplast intrinsic protein1;3-1* (*tip1;3-1*) and *tip3;1* of vacuole-specific aquaporins, *sand-2*/*monensin sensitivity1* that causes vacuole fragmentation, and the double mutant of na^+/h^+ *exchanger1-2* (*nhx1-2*) and *nhx2-1* that affects potassium uptake into vacuoles. (B) Series of longitudinal sections of WT and *sgr2-1* from egg cells to globular embryos. Egg cells are outlined, and orange arrowheads indicate the large spherical vacuoles. (C) Frequency of the abnormal globular embryos, in which cell division pattern was different from WT. (D) Seven-day-old seedlings of WT and *sgr2-1*. The appearance of tricot seedlings is shown (0/320 in WT and 12/355 in *sgr2-1*; $p < 0.01$ by Fisher's exact test). Scale bars: 20 µm (A and B) and 1 mm (D).

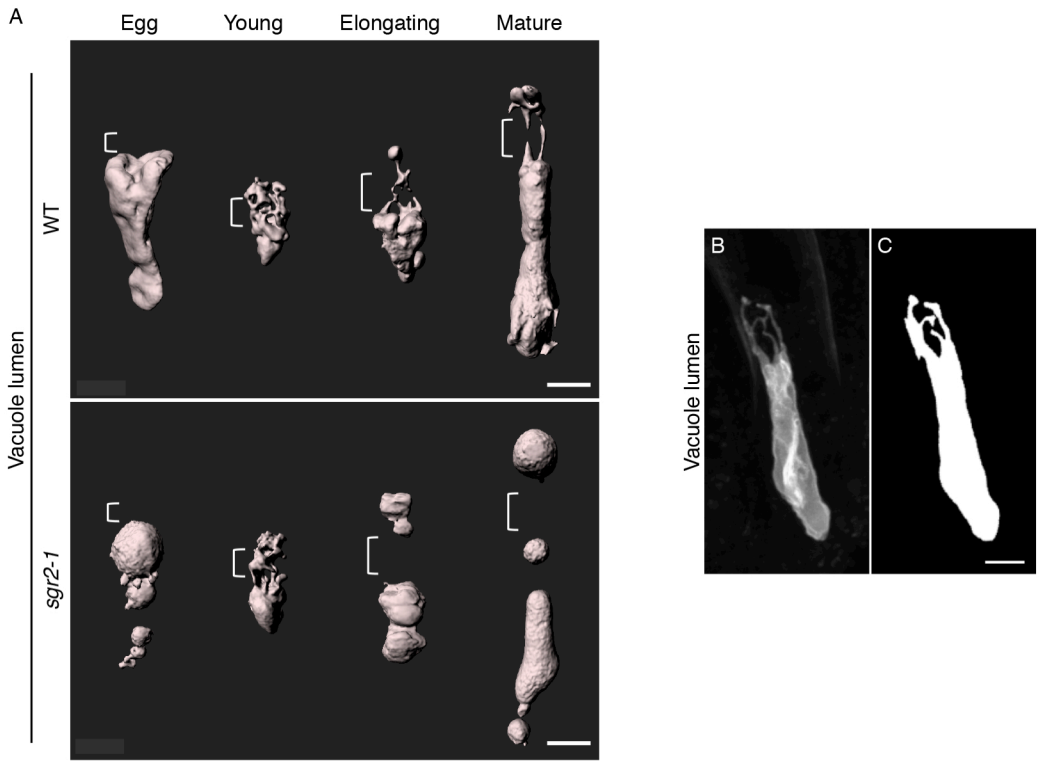

Fig. S2. Three-dimensional (3D) images and image quantification of vacuoles.
(A) The 3D-reconstructed images of vacuoles at the egg cell and indicated zygotic stages. Images were generated using the vacuolar lumen marker. Brackets show the perinuclear area. (B and C) Image processing of 2PEM images of the WT mature zygotes expressing the vacuolar lumen marker for the morphometry of the vacuole. (B) MIP image generated by serial optical sections. (C) Binary image of the vacuole of B. Scale bars: 10 μm.

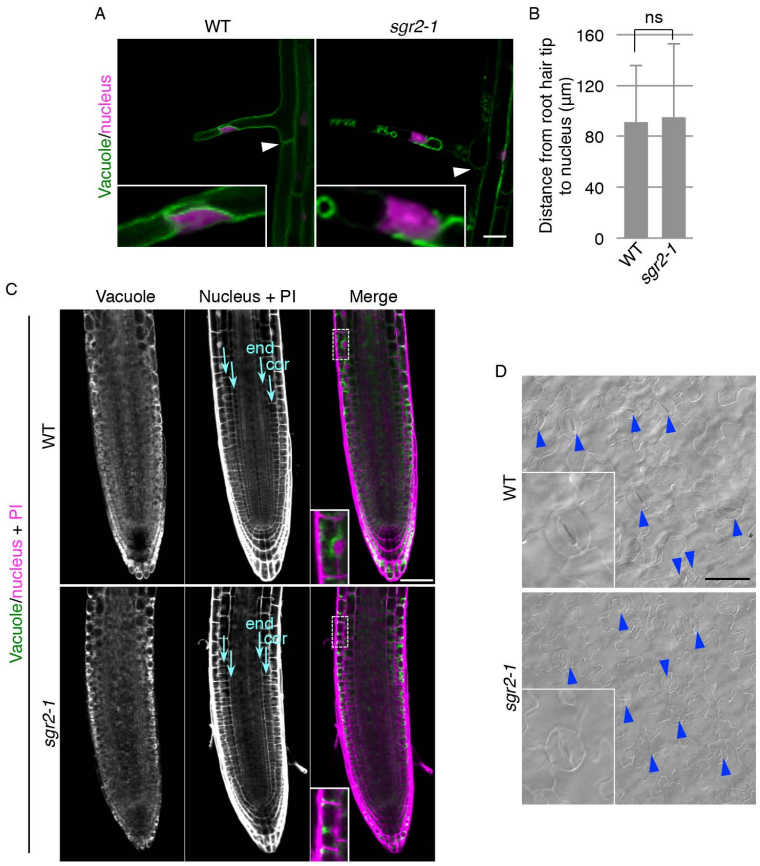

Fig. S3. The effect of *sgr2-1* in postembryonic organs.
(A) Confocal images of root hairs in five-day-old seedlings. Root tips point to the lower side of the pictures, and arrowheads show the lower end of the cell, indicating that root hairs emerged at the basal end of the epidermal cell both in WT and *sgr2-1*. Insets display enlarged images of the perinuclear region. (B) Graph of the distance from the root hair tip to the center of the nucleus, denoted as the cell polarity, in the mature root hairs of ten-day-old seedlings. Error bars represent the SD [N = 17 (WT) and 13 (*sgr2-1*)], and significant difference from the WT value was determined by two-sided Student's *t* test. Ns = not significant. (C) Confocal images of PI-stained root meristems in five-day-old seedlings expressing the vacuolar/nuclear marker. WT and *sgr2-1* both showed well-organized cell layers (cyan arrows), including the cortex (cor) and the endodermis (end), which were generated by the asymmetric cell division of the unique initial cell. Insets display the enlarged images of the dotted square areas, showing the large spherical vacuoles in *sgr2-1*. (D) DIC images of five-day-old abaxial cotyledons. Arrowheads indicate the stomata, which are uniformly distributed both in WT and *sgr2-1*. Insets display the enlarged images of the stomata, showing that the stomatal morphology was indistinguishable between WT and *sgr2-1*. Scale bars: 20 μm (A) and 50 μm (C and D).

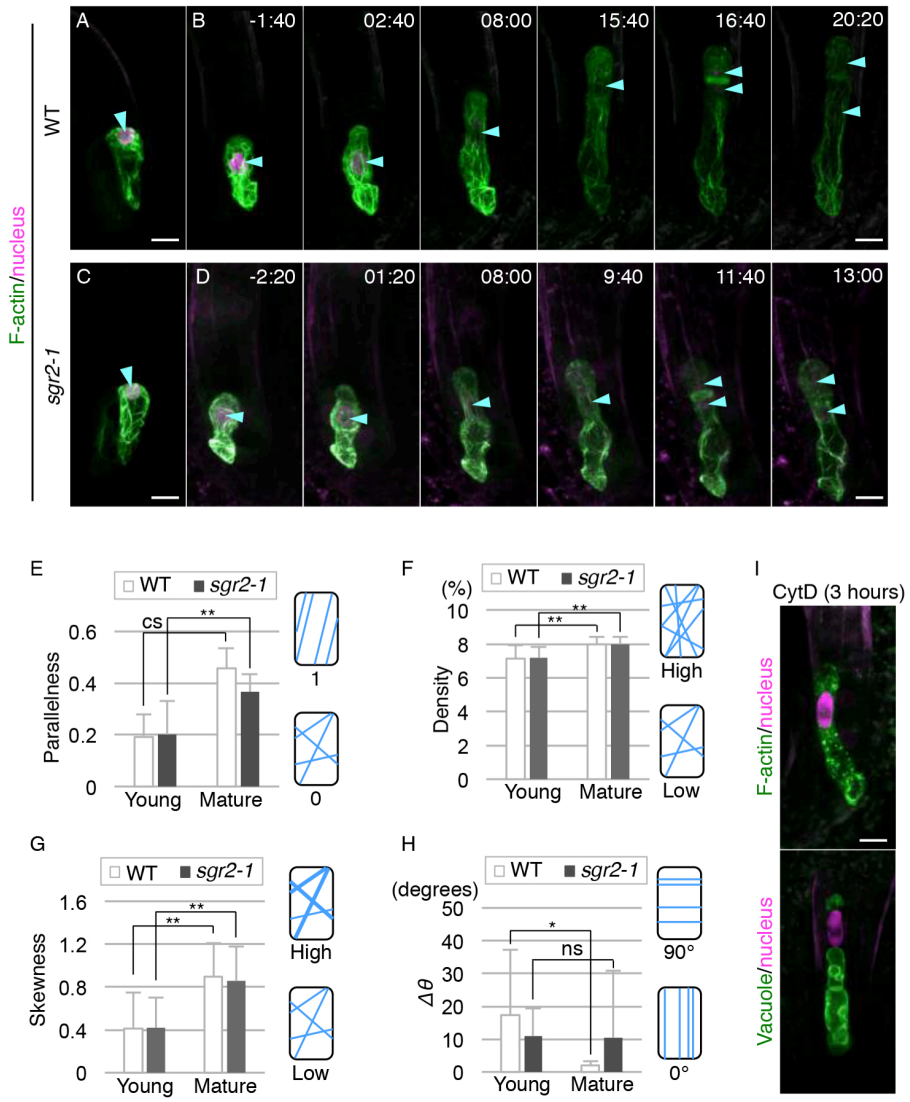

Fig. S4. Live-cell imaging and quantification of F-actin dynamics in the zygote.
(A-D) 2PEM images of the egg cell (A and C) and the time-lapse observations of the zygote in *in vitro*-cultivated ovules (B and D) expressing the F-actin/nuclear marker. MIP images are shown. Images are representative of 10 (WT) and 5 (*sgr2-1*) time-lapse images, respectively. Numbers indicate the time (h:min) from bulging, and cyan arrowheads indicate the nuclei. (E-H) Graphs of the parallelness (E), density (F), skewness of the intensity distribution (a metric for the appearance of bundled cables) (G), and average angle of the fibers against the cell longitudinal axis ($\Delta\theta$; H) of F-actin in the indicated cells. Data sets of mature zygotes in E and H correspond to the values of 'whole cell' in Figure 4E and 4F, respectively, because these measurements were performed in a single experiment. Error bars represent the SD [N = 10 (WT, Young), 12 (WT, Mature), 10 (*sgr2-1*, Young) and 13 (*sgr2-1*, Mature)], and significant differences from the values of respective young zygotes were determined by Brunner–Munzel test; cs, complete segregation; **, $p < 0.01$; *, $p < 0.05$; Ns = not significant. Illustrations show the correlations between the respective values and the fiber patterns. (I) 2PEM images of the mature zygotes expressing the F-actin/nuclear and vacuolar/nuclear markers after exposure to the polymerization inhibitor of F-actin (100 µM CytD) for 3 hours. Scale bars: 10 µm.

Movie S1. Vacuole dynamics from the young zygote to the first cell division in wild type (WT).
Time-lapse observation of the vacuolar/nuclear marker in the WT zygote. Numbers indicate the time (h:min) from the bulging. MIP images are shown, and images were obtained at 20-min intervals. Scale bar: 10 μm.

Movie S2. Vacuole dynamics from the young zygote to the first cell division in *sgr2-1*.
Time-lapse observation of the vacuolar/nuclear marker in the *sgr2-1* zygote. Numbers indicate the time (h:min) from the bulging. MIP images are shown, and images were obtained at 20-min intervals. Scale bar: 10 μm.

Movie S3. F-actin dynamics from the young zygote to the first cell division in WT.
Time-lapse observation of the F-actin/nuclear marker in the WT zygote. Numbers indicate the time (h:min) from the bulging. MIP images are shown, and images were obtained at 20-min intervals. Scale bar: 10 μm.

Movie S4. F-actin dynamics from the young zygote to the first cell division in *sgr2-1*.
Time-lapse observation of the F-actin/nuclear marker in the *sgr2-1* zygote. Numbers indicate the time (h:min) from the bulging. MIP images are shown, and images were obtained at 20-min intervals. Scale bar: 10 μm.

References

1. Kato T, et al. (2002) SGR2, a phospholipase-like protein, and ZIG/SGR4, a SNARE, are involved in the shoot gravitropism of *Arabidopsis*. *Plant Cell* 14(1):33-46.
2. Ebine K, et al. (2014) Plant vacuolar trafficking occurs through distinctly regulated pathways. *Curr Biol* 24(12):1375-1382.
3. Peiter E, et al. (2005) The vacuolar Ca2+-activated channel TPC1 regulates germination and stomatal movement. *Nature* 434(7031):404-408.
4. Mao Z, Sun W (2015) *Arabidopsis* seed-specific vacuolar aquaporins are involved in maintaining seed longevity under the control of ABSCISIC ACID INSENSITIVE 3. *J Exp Bot* 66(15):4781-4794.
5. Wudick MM, Luu DT, Tournaire-Roux C, Sakamoto W, Maurel C (2014) Vegetative and sperm cell-specific aquaporins of *Arabidopsis* highlight the vacuolar equipment of pollen and contribute to plant reproduction. *Plant Physiol* 164(4):1697-1706.
6. Barragan V, et al. (2012) Ion exchangers NHX1 and NHX2 mediate active potassium uptake into vacuoles to regulate cell turgor and stomatal function in *Arabidopsis*. *Plant Cell* 24(3):1127-1142.
7. Sprunck S, et al. (2012) Egg cell-secreted EC1 triggers sperm cell activation during double fertilization. *Science* 338(6110):1093-1097.
8. Segami S, Makino S, Miyake A, Asaoka M, Maeshima M (2014) Dynamics of vacuoles and H+-pyrophosphatase visualized by monomeric green fluorescent protein in *Arabidopsis*: artifactual bulbs and native intravacuolar spherical structures. *Plant Cell* 26(8):3416-3434.
9. Kawashima T, et al. (2014) Dynamic F-actin movement is essential for fertilization in *Arabidopsis thaliana*. *Elife* 3.
10. Steffen JG, Kang IH, Macfarlane J, Drews GN (2007) Identification of genes expressed in the *Arabidopsis* female gametophyte. *Plant J* 51(2):281-292.
11. Voelz R, Heydlauff J, Ripper D, von Lyncker L, Gross-Hardt R (2013) Ethylene signaling is required for synergid degeneration and the establishment of a pollen tube block. *Dev Cell* 25(3):310-316.

12. Kimata Y, et al. (2016) Cytoskeleton dynamics control the first asymmetric cell division in *Arabidopsis* zygote. *Proc Natl Acad Sci U S A* 113(49):14157-14162.
13. Ueda M, Zhang Z, Laux T (2011) Transcriptional activation of *Arabidopsis* axis patterning genes *WOX8/9* links zygote polarity to embryo development. *Dev Cell* 20(2):264-270.
14. Hajdukiewicz P, Svab Z, Maliga P (1994) The small, versatile pPZP family of Agrobacterium binary vectors for plant transformation. *Plant Mol Biol* 25(6):989-994.
15. Curtis MD, Grossniklaus U (2003) A gateway cloning vector set for high-throughput functional analysis of genes in planta. *Plant Physiol* 133(2):462-469.
16. Adachi S, et al. (2011) Programmed induction of endoreduplication by DNA double-strand breaks in *Arabidopsis*. *Proc Natl Acad Sci U S A* 108(24):10004-10009.
17. Vitale A, Raikhel NV (1999) What do proteins need to reach different vacuoles? *Trends Plant Sci* 4(4):149-155.
18. Clough SJ, Bent AF (1998) Floral dip: a simplified method for Agrobacterium-mediated transformation of *Arabidopsis thaliana*. *Plant J* 16(6):735-743.
19. Kurihara D, Kimata Y, Higashiyama T, Ueda M (2017) In Vitro Ovule Cultivation for Live-cell Imaging of Zygote Polarization and Embryo Patterning in *Arabidopsis thaliana*. *J Vis Exp* (127).
20. Higaki T, Kutsuna N, Okubo E, Sano T, Hasezawa S (2006) Actin microfilaments regulate vacuolar structures and dynamics: dual observation of actin microfilaments and vacuolar membrane in living tobacco BY-2 Cells. *Plant Cell Physiol* 47(7):839-852.
21. Brunner E, Munzel U (2000) The nonparametric Behrens-Fisher problem: Asymptotic theory and a small-sample approximation. *Biometrical Journal* 42(1):17-25.